ADVANCED FUNCTIONAL MATERIALS
www.afm-journal.de

Unraveling the Role of Spacer Cations: Toward Constructing Ideal Dion–Jacobson Halide Perovskites

Zhengxun Lai, Yi Shen, Bei Jiang, Yuxuan Zhang, You Meng, Di Yin, Boxiang Gao, Weijun Wang, Pengshan Xie, Yan Yan, SenPo Yip, Lei Liao, and Johnny C. Ho**

Dion–Jacobson-type 2D halide perovskites (DJPs) present an ideal alternative to their 3D counterparts due to their superior stability and exceptional optoelectronic properties. Despite the numerous DJPs proposed in recent years, the impact of different spacer cations on DJPs remains unclear. This understanding is crucial for researchers to select suitable materials and is an urgent requirement for the development of higher-performance DJPs-based devices. In this study, the influence of the chain-like spacer cations with varying branch chains and chain lengths is thoroughly examined using both theoretical and experimental methods. The findings reveal that spacer cations with high polarity components along the main chain direction enhance the stability and photoelectric properties of DJPs. Additionally, it is found that the chain length of the spacer cation plays a critical role. Chain lengths that are too long or too short can detrimentally affect the photoelectric performance and stability of DJPs. These insights will guide researchers in selecting suitable spacer cations and in innovating new types of DJPs.

1. Introduction

The past decade has seen a surge of interest in halide perovskites due to their excellent optoelectronic performance.[1–6] This captivating material has now moved beyond the confines of the laboratory and is progressively being utilized in industrial production. However, as halide perovskites venture toward industrial output and commercialization, they are encountering a host of challenges.[7–10] To address future issues, a fundamental understanding of the inherent structures and properties of different types of halide perovskites is essential. The conventional 3D halide perovskites follow the chemical formula ABX_3, where "A" represents a large alkali metal like Rb and Cs or short-chain ammonium, such as methylamine (MA) or formamidine, "B" denotes a transition metal element like Sn or Pb, and "X" symbolizes a halogen. Despite their potential, the stability of the 3D halide perovskites is poor, rendering them unsuitable for use in ambient environments.[11,12] To enhance the stability of 3D halide perovskites, long-chain organic molecules are incorporated to form 2D halide perovskites. Currently, there are three types of 2D halide perovskites: the Dion–Jacobson, Ruddlesden–Popper, and alternating cation in the interlayer space types.[13–15] Among these, the Dion–Jacobson type 2D halide perovskites (DJPs) show the most promise, exhibiting greater stability and superior optoelectronic performance due to their advanced lattice structure, devoid of weak van der Waals bonds.[16,17] The chemical formula of DJPs is defined as $LA_{n-1}B_nX_{3n+1}$, where A, B, and X are consistent with the 3D counterparts, and L represents a long-chain organic molecule, known as a spacer cation, which separates n layers of PbI_6 octahedra. In recent years, significant advancements have been made in the field, with various types of DJPs and their corresponding devices being reported.[18,19] For instance, Niu et al. fabricate solar cells with the DJPs based on 1,4-butanediamine cations, achieving an enhanced power conversion efficiency compared to the RPP-based ones.[20] Zheng et al. also achieved a high-sensitivity X-ray imager with Dion–Jacobson and Ruddlesden–Popper halide perovskites, which is promising for next-generation low-dimensional X-ray detectors.[21,22] Yang et al. fabricated 2D/3D halide perovskites with amidino-based spacer cations. The 2D DJP component decreased the concentrations of voids and bulk defects of the

Z. Lai, B. Jiang, L. Liao
Changsha Semiconductor Technology and Application Innovation Research Institute
College of Semiconductors (College of Integrated Circuits)
Hunan University
Changsha 410082, China
E-mail: liaolei@whu.edu.cn

Y. Shen, Y. Zhang, Y. Meng, D. Yin, B. Gao, W. Wang, P. Xie, Y. Yan, J. C. Ho
Department of Materials Science and Engineering
City University of Hong Kong
Kowloon, Hong Kong SAR 999077, China
E-mail: johnnyho@cityu.edu.hk

Y. Meng, J. C. Ho
State Key Laboratory of Terahertz and Millimeter Waves
City University of Hong Kong
Kowloon, Hong Kong SAR 999077, China

S. Yip, J. C. Ho
Institute for Materials Chemistry and Engineering
Kyushu University
Fukuoka 816–8580, Japan

The ORCID identification number(s) for the author(s) of this article can be found under https://doi.org/10.1002/adfm.202409987

DOI: 10.1002/adfm.202409987

perovskite films, leading to high-performance solar cells with a high power conversion efficiency of up to 24.9%.[23] Kanatzidis et al. designed mixed Pb/Sn DJPs (3AMPY) $(MA)_{n-1}Pb_xSn_{n-x}Br_{3n+1}$ (3AMPY = 3-(aminomethyl) pyridinium), which exhibit desirable low bandgaps beneficial to optoelectronic applications.[24] They also found that the position of amino groups of aromatic diammonium cations can lead to the distortion of the Pb-I octahedra and contribute to broader white-light emission of the DJPs.[25] Despite these advancements, there is still considerable work to be done to realize high-performance, long-term stable DJPs and fully industrialize this promising material. Importantly, a comprehensive understanding of how spacer cations impact the stability and device performance of different DJPs is still lacking. This knowledge is crucial for the study and development of next-generation DJPs. Therefore, it is both essential and urgent to investigate the influence of different organic spacers on DJPs.

In this study, we aim to address the development challenges of halide perovskites demonstrated above, particularly the DJPs. We systematically investigate the impact of various spacer cations on DJPs using both theoretical and experimental methods. Our findings reveal that the polarity of spacer cations significantly influences the stability and photoelectric properties of DJPs. A spacer cation with a larger polarity component along the main chain direction can effectively enhance the stability and photoelectric device performance of DJPs. Additionally, the chain length of the spacer cation also plays a pivotal role. As the chain length increases, the stability of the DJP structure initially improves, then weakens, suggesting that an optimal chain length is crucial for achieving satisfactory device performance. These results provide a systematic understanding of the influence of spacer cations on DJPs, offering valuable insights to researchers for the design and selection of suitable spacer cations and the development of new types of DJPs.

2. Results and Discussion

For the long-chain diamine-based spacer cation of DJPs, its feature can be defined by its chain length and branch chains. It needs to be pointed out that to simplify the study, we only focus on the chain-like spacer cations without aromatic rings in this work. Some aromatic rings can also be incorporated into some spacer cations, but they can also be seen as branch chains, which is not included in this work.[26,27] For the chain-like spacer cations of the DJPs, their chain length can be determined by the number of C atoms in the main chain between these two amines. As shown in **Figure 1**a, the number of C atoms in methanediamine (MDA) is 1, in ehylendiamine (EDA) is 2, and in propanediamine (PDA) is 3. Herein, we will first investigate the role of branch chains in DJPs and their influence on the stability and optoelectronic properties by first-principle calculations. As for the branch chain, we use PDA as the base molecule and gradually add branch chain alkyls to it (Figure 1b). Then, different spacer cations can be obtained: N-Methyl-1,3-propanediamine (MPDA), 3-Dimethylaminopropylamine (DMPA), N,N′-Dimethyl-1,3-propanediamine (DMPDA), N,N,N′-Trimethyl-1,3-propanediamine (TMPDA). From these derived spacer cations from PDA in Figure 1b, one can find that PDA and DMPDA are perfectly symmetric; for DMPA, there

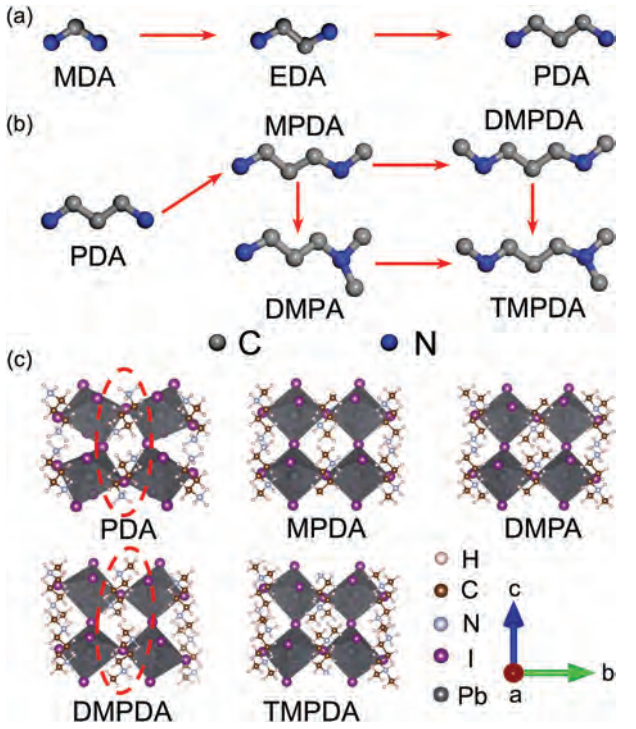

Figure 1. Schematics of spacer cations with a) different chain lengths and b) different branch chains, where the hydrogen atoms are hidden. c) Optimized structures of the DJPs with the spacer cations in b).

are two groups of alkyls on one side of PDA, the asymmetry of which is larger than that of MPDA (one group of alkyl on the one side of PDA) and TMPDA (one group of alkyl on the one side and two group of alkyl on the other side of PDA). Therefore, the degree of symmetry of these spacer cations can be acquired: PDA, MPDA > DMPDA, TMPDA > DMPA.

After the construction of the spacer cations, 2D DJPs with the n value of 1 are constructed using these spacer cations, and the lattice and physical properties are detailly studied and compared. It needs to be pointed out that to exclude the influence of the n value, 2D DJPs (n = 1, with the molecular formula of $LPbI_4$, L represents the spacer cations) are chosen in this work. Another important reason to choose the DJPs with the n value of 1 is that when n>1, the film fabricated experimentally is a mixed phase, which is not conducive to this study.[28] Besides, to construct the DJ phase structure with the spacer cations mentioned above, we first designed and built the original lattice structures. After that, we performed lattice optimization on the structures with low energy and atomic convergent forces (Experimental Section). The systems were convergent and maintained the DJ-type structure after the optimization, ensuring the formation of DJ phases. Figure 1c depicts the lattice structure of the DJPs after the lattice optimization, where these DJPs are referred to as their corresponding spacer cations below, i.e., PDA, MPDA, DMPA, DMPDA, and TMPDA. One can see a slight distortion of the DMPDA lattice and a blatant distortion of the PDA lattice, where one can also notice that both PDA and DMPDA spacer cations are symmetric. The distorted lattice can lead to their relatively poor stability. Accordingly, the stability of these DJPs is studied first.

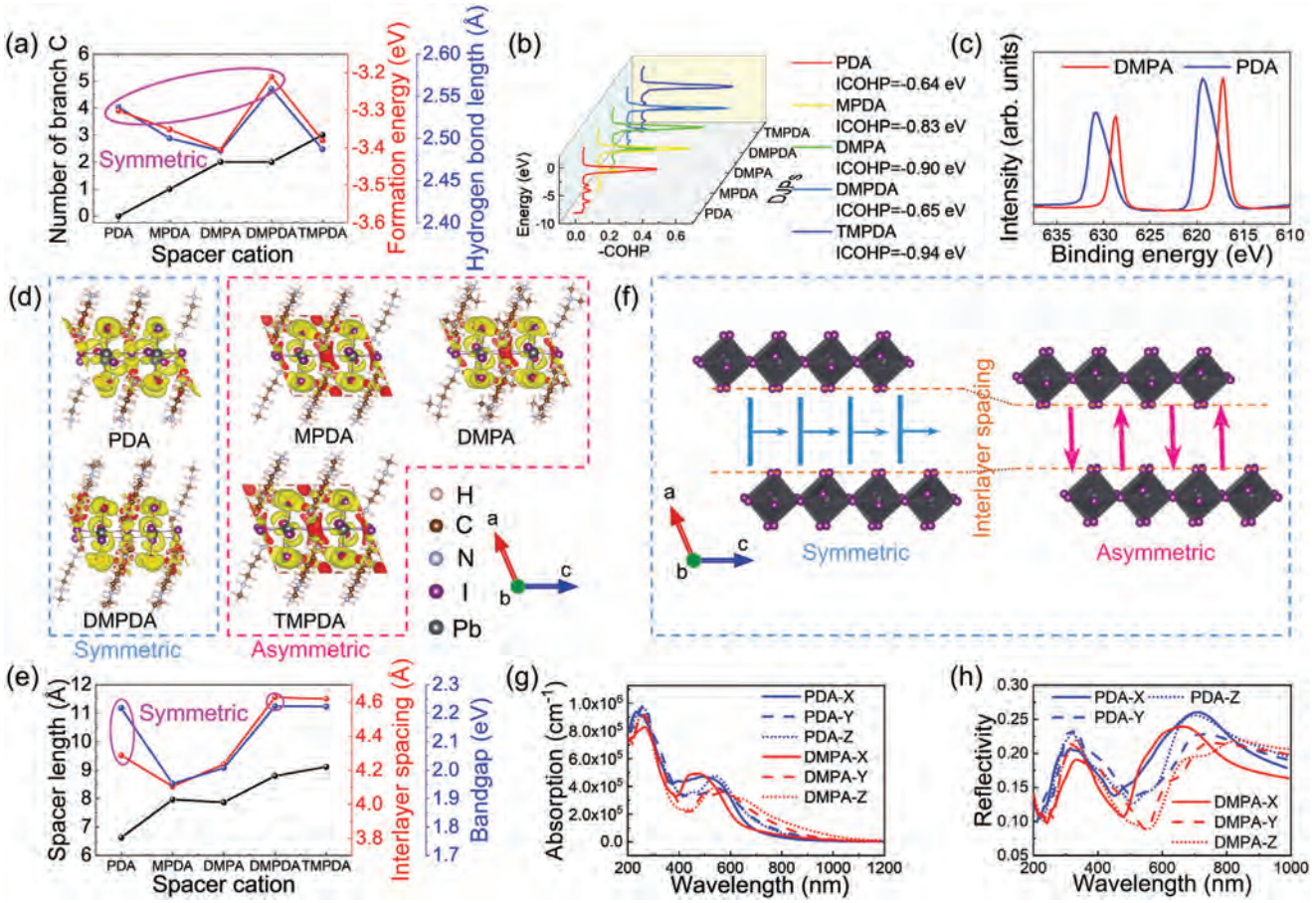

Figure 2. a) The number of branch C, formation energies and the length of the hydrogen bonds in the DJPs. b) The COHP and the ICOHP values of the DJPs. c) I 3d XPS spectra for the DMPA and PDA perovskite films. d) Charge density difference maps of the DJPs with different branch chains viewing along the *b* axis. e) The length of the spacer cations, interlayer spacings, and bandgaps of the DJPs. f) The schematics of the DJPs' lattice structures with symmetric and asymmetric spacer cations, respectively. g) Absorption and h) reflectivity spectra of DMPA and PDA acquired by DFT calculations.

We use formation energy to characterize their stability. Since the DJPs are fabricated experimentally using these precursors: the spacer cations, PbI_2 and HI, the formation energy can be defined as $E_0 = E_{DJP} - E_{Spacer} - E_{PbI} - E_{HI}$, where E_{DJP}, E_{Spacer}, E_{PbI}, and E_{HI} are the internal energies of the DJPs, spacer cations, PbI_2 and HI, respectively. The calculated formation energies of these DJPs are shown in **Figure** 2a, where the left axis shows the number of the branch alkyls of the spacer cations. Notably, the formation energy has no direct relation with the number of branch alkyls. The DJPs PDA and DMPDA with symmetric spacer cations show larger formation energies, which confirms their poor stability compared with the other asymmetric ones. To visually illustrate the symmetry of these spacer cations, the dipole moments of them were also calculated and presented in Figure S1 (Supporting Information). For the symmetric spacer cations PDA and DMPDA, the direction of the dipole moments is perpendicular to the main chain of the molecules. However, for the asymmetric MPDA, DMPA, and TMPDA, the dipole moments lean to the side with more branch alkyls. Especially for DMPA, the asymmetry is the largest as demonstrated above. This observation can also be confirmed by its largest dipole moment of 2.95 D with the direction even parallel to the main chain. Therefore, we can suppose that the dipole moment component along the main chain direction can strengthen the hydrogen bond between the spacer cation and the inorganic layers, enhancing the stability of the DJPs with asymmetric spacer cations, just as Figure 2a shows. Accordingly, the crystal orbital Hamilton population (COHP) analysis between the I and H atoms was carried out, which can provide the strength of the hydrogen bonds directly (Figure 2b).[29] Evidently, all the states of the I–H atoms of these DJPs below the Fermi level are the binding states, contributing to their stable structures. The integrated COHP (ICOHP) of these samples is also labeled in the figure. The binding states of the DJPs PDA (ICOHP = −0.64 eV) and DMPDA (ICOHP = −0.65 eV) with symmetric spacer cations are obviously less than those of the asymmetric ones (ICOHP = −0.83, −0.90, and −0.94 eV). The COHP analysis results confirm the stronger hydrogen bonds in these "asymmetric" DJPs. Additionally, a shorter hydrogen bond generally means it is stronger. The average length of the hydrogen bonds in the DJPs is also shown in Figure 2a, corresponding to their formation energy, confirming the hydrogen bonds' crucial role. To experimentally verify the enhanced hydrogen bonds in the "asymmetric" DJPs, the PDA and DMPA DJP films with respectively symmetric and asymmetric spacer cations

Table 1. Lattice parameter *a* and Pb–I–Pb angles of the DJPs.

DJP	Lattice parameter *a* [Å]	Pb-I-Pb angle 1 [deg]	Pb-I-Pb angle 2 [deg]	Average value [deg]
PDA	11.77	133.51	157.43	145.47
MPDA	11.45	155.56	174.33	164.95
DMPA	11.48	152.97	171.87	162.42
DMPDA	11.83	134.71	155.17	144.94
TMPDA	11.66	147.72	169.05	158.39

were fabricated by spin-coating method, and X-ray photoelectron spectroscopy (XPS) measurement was conducted to them. As illustrated in Figure 2c, the binding energy of I 3d in DMPA shifts to a lower value than PDA, which is attributed to the stronger I–H hydrogen bonds.[30,31] Besides, one can see the line width of the PDA XPS peaks is much larger than that of DMPA, indicating the different chemical bonding of I atoms in PDA caused by the structural distortion. To demonstrate how the hydrogen bonds are strengthened in the DJPs' lattice, the charge density difference maps of these DJPs were also simulated and presented in Figure 2d and Figure S2 (Supporting Information), where the yellow and red regions represent the accumulation and depletion of electrons, respectively. The red areas in the "asymmetric" DJPs' lattices are larger, indicating more electron transfer caused by the polarity of the asymmetric spacer cations. All these results suggest that a spacer cation with a large polarity component along the main chain direction can effectively enhance the stability of the DJPs by both strengthening the hydrogen bonds and reducing the distortion of the lattice.

Figure 2e shows the bandgap, interlayer spacing, and spacer length (the molecule length of the spacer cation) of the DJPs. The interlayer spacing is supposed to correlate positively with the chain length of the spacer cation. However, one can see in Figure 2e that it does not increase as the spacer length increases: although the chain length of the symmetric PDA and DMPDA spacers are not the largest, their interlayer spacings are even larger than the asymmetric ones with longer chain length. This discovery indicates that a spacer cation with high polarity along the main chain direction can decrease the interlayer spacing, making the DJP crystals more compact. To visually demonstrate this conclusion, the schematics of DJPs' lattice structures with symmetric and asymmetric spacer cations are illustrated in Figure 2f. For the asymmetric ones, the much higher polarity along the main chain direction will strengthen the hydrogen bonds between the spacer cations and the inorganic layers, and at the same time, draw the inorganic layers close. For the strictly symmetric ones, because the polarization is perpendicular to the molecule, the polarization will interact more with each other but not the inorganic layers, leading to larger interlayer spacings and distorted inorganic layers, which further affects the stability of the DJPs, as demonstrated in Figure 1c. The distortion of the inorganic layer can also be compared directly by the two Pb–I–Pb angles, as is shown in Figure S3 (Supporting Information), where the ideal Pb–I–Pb angle is 180°.[32,33] As is shown in **Table 1**, the lattice parameter *a* (the lattice parameter perpendicular to the stacked layers) and the two Pb–I–Pb angles of these DJPs are listed. One can see that the change of the lattice parameter *a* is consistent with the interlayer spacings: symmetric PDA and DMPDA are larger than asymmetric MPDA, DMPA, and TMPDA. Expectedly, the Pb–I–Pb angles of PDA and DMPDA distorted more extensively than those of MPDA, DMPA, and TMPDA, contributing to the poor stability of PDA and DMPDA-based DJPs. The stability of the symmetric PDA and asymmetric DMPA-based DJPs was also studied using molecular dynamics simulation through ab initio molecular dynamic (AIMD) calculation with VASP (Figure S4a, Supporting Information). The temperature was set at 100 °C (373 K) in the simulation. For asymmetric DMPA, the atoms vibrate near their original location. However, for symmetric PDA, the lattice started to decompose after 10 ps. The energies of these two systems are also delineated in Figure S4b (Supporting Information). It is expected that the total energy of DMPA remains stable, but the energy of PDA has a sharp increase at 10 ps. The AIMD results confirm the superior stability of the DJPs with asymmetric cations.

Apart from the stability of the halide perovskites, their optoelectronic properties also need our attention, which is significant to the performance of the optoelectronic devices. The interlayer spacing of these DJPs is supposed to be related to the quantum confinement effect. This way, one can see in Figure 2e that the changes in the bandgaps of these DJPs are strictly consistent with the interlayer spacing caused by the quantum confinement effect, indicating the bandgaps are mainly determined by the interlayer spacings.[34,35] The band structures of these DJPs are also shown in Figure S5 (Supporting Information). The fundamental bandgaps of them all appear at a Γ high symmetry point. It is evident that different from the DJPs PDA and DMPDA with symmetric spacer cations, there is substantial overlap between Pb and I atomic orbitals in the other three (marked by red circles), which can reduce the bandgap. The result suggests that the distortion of the lattice structures of the symmetric spacer cations-based DJPs also plays a crucial role in enlarging their bandgaps. In addition, the narrowed interlayer spacing of the DJPs with asymmetric spacer cations will also be supposed to alleviate the obstruction of electronic transmission along the layer-stacking direction in 2D halide perovskite and further enhance the optoelectronic performance. Therefore, the optical properties of these DJPs with symmetric spacers PDA and asymmetric spacers DMPA were studied by first-principle calculations. Figure 2g displays their absorption spectra. The absorption edge of DMPA has a red shift compared to PDA due to the smaller bandgap. The reflectivity of DMPA is visibly smaller than that of PDA (Figure 2h), which is favorable in optoelectronic devices to increase efficiency. The dielectric constant and conductivity of the DJPs are also shown in Figure S6 (Supporting Information). The DJPs with symmetric spacer cations show larger dielectric constants and conductivities, benefiting from the spacer cations' larger polarities, which can contribute to the transport of the carriers.

To further prove the results acquired by the first-principle calculations above, the DJP films with symmetric spacers PDA and asymmetric spacers DMPA were also used to study their stability and optoelectronic performance experimentally. As we have mentioned, the DJP films with n = 1 phase are chosen in this work because of their pure-phase nature. The films were first characterized by X-ray diffraction (XRD) (**Figures 3**a,d). Their XRD patterns are consistent with the simulation ones, further confirming the pure-phase DJP films. The scanning electron

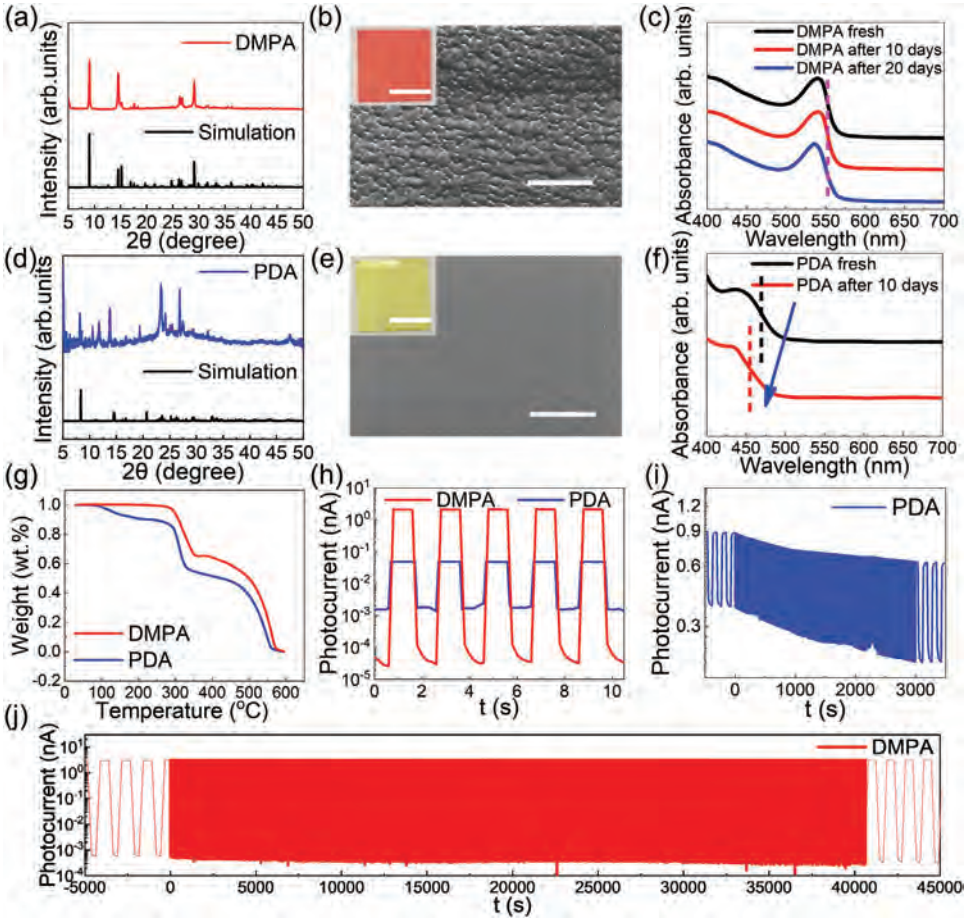

Figure 3. Experimental results of the DMPA and PDA films and photodetectors. XRD curves and the corresponding simulation results of a) DMPA and d) PDA films. The SEM images of b) DMPA and e) PDA films (the scale bars are both 50 μm), where the insets are their optical pictures (the scale bars are both 10 mm). Absorption spectra of c) DMPA and f) PDA films after a long time storage. g) TGA curves of the DMPA and PDA films. h) I–t curves of the DMPA and PDA-based photodetectors under the illumination of the chopped laser. Long-time operation of the i) PDA and j) DMPA films-based photodetectors with continuous on–off switching.

microscope (SEM) image of the DMPA film (Figure 3b) suggests that its grains are larger than 10 μm, indicating its good crystallinity. The PDA film also shows a smooth surface (Figure 3e). From their optical images in the insets, one can see that the DMPA film is orange and the PDA film is yellow, which results from the smaller bandgap of DMPA than PDA. Their thicknesses can also be acquired by the cross-sectional SEM images in Figure S7 (Supporting Information), where the thickness of DMPA and PDA films is ≈909 and 788 nm, respectively. Next, the stability of these two DJP films was studied. Figures 3c,f show the absorption spectra of the DJP films before and after storage in a humid environment (the humidity is ≈70%). After 20 days of storage, the absorption spectrum of DMPA films remained unchanged, suggesting its excellent long-term stability. However, for the PDA film, the absorption edge blue shifted from 469 to 455 nm, indicating the decomposition of the PDA film remaining the inorganic PbI_2 residue. The thermal stability of the films was also studied by thermogravimetric analysis (TGA) (Figure 3g). The PDA film started to decompose at the temperature of 90 °C. However, for DMPA film, the decomposition temperature was as high as 270 °C, confirming its much better thermal stability. In addition, the DJP films were also configured into photodetectors to further investigate their performance and operation stability in devices, which is significant for their future application. Figure 3h shows the on–off switching curves of the photodetectors under a 450-nm laser. It is evident that both the photocurrent and on/off ratio of the DMPA-based photodetector is much larger than that of PDA, confirming the better optoelectronic properties of DMPA. The long-term on/off switching stability of the photodetectors was then studied: these two photodetectors were put into continuous operation with a bias voltage of 1.5 V and the illumination of a chopped laser (Figures 3i,j). The wavelength of the laser was 450 nm with a fixed light intensity of 100 mW cm^{-2}. One can see the photocurrent of the PDA-based photodetector gradually decreased during the operation. On the other hand, for DMPA, the photodetector could keep stable without any decay for more than 40 000 s. The experimental results confirm the superior stability and optoelectronic performance of the asymmetric spacer cations-based DJPs.

As demonstrated above, apart from the branch chain, the main chain length is also a main factor of the spacer cation, as shown in

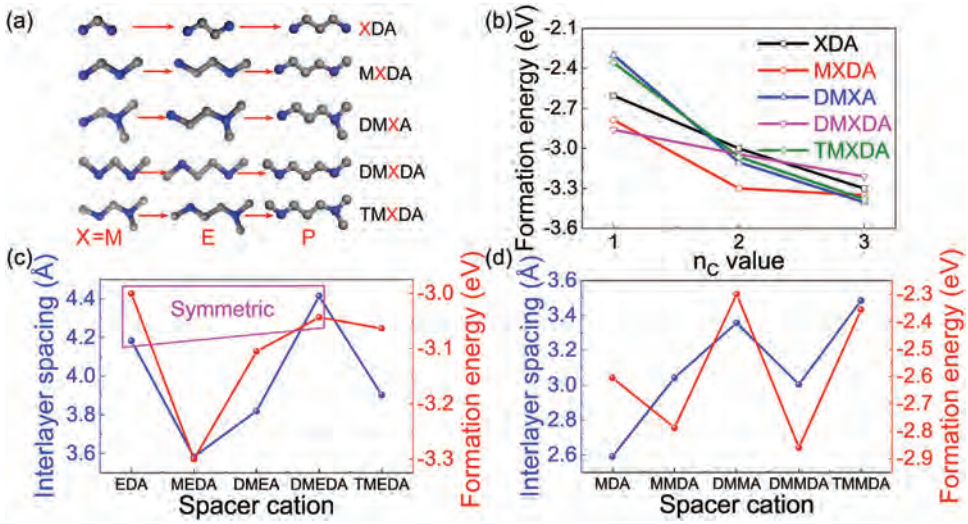

Figure 4. a) Schematics of spacer cations with different chain lengths and branch chains. b) Formation energies of all the DJPs in a). Interlayer spacings and formation energies of the DJPs constructed by the spacer cations with the n_C value of c) two and d) one.

Figure 1a. Hence, the influence of the main chain length on DJPs is then investigated in detail. We use n_C to represent the number of C atoms between the two amino groups in the spacer cations. The n_C values of the spacer cations we studied above in Figure 1b are all three. In these cases, there is a letter "P" in their abbreviations, PDA, MPDA, DMPA, DMPDA, and TMPDA, representing "propyl", which comes from the n_C value three. Accordingly, when we reduce the n_C value to two and one, the letters "E" and "M" can be used to represent ethyl and methyl. As depicted in **Figure** 4a, these derived DJPs can be referred to as XDA, MXDA, DMXA, DMXDA, and TMXDA, where X represents M, E, or P. Figure 4b shows the formation energies of the DJPs. One can see that for all these DJPs with different branch chains, the formation energy decreases as the chain length increases, suggesting enhanced stability. However, it needs to be pointed out that when the n_C value comes to four, DMXDA perovskite cannot maintain a stable lattice, indicating that a symmetric spacer cation with a much longer chain is harmful to the stability of DJPs. To thoroughly study the effect of chain length on the spacer cations, the interlayer spacings and formation energies of the DJPs with n_C values of two and one are also presented (Figures 4c,d). Similar to the n_C value of three discussed above, for the DJPs with the n_C value of two, the DJPs with symmetric spacer cations EDA and DMEDA show the highest formation energies and largest interlayer spacings, which is attributed to their zero component of polarity along the main chain direction as we demonstrated above. However, the DJPs with n_C value of one in Figure 4d differ from those with n_C values of two and three, where the symmetric MDA and DMMDA no longer show the highest formation energies. It is because these spacer cations with $n_C = 1$ are too small, and are even able to act as the A site cations in 3D halide perovskites. These small spacer cations can excessively reduce the interlayer spacings, which will acutely twist the lattice of the DJPs. The length of the hydrogen bonds of $n_C = 1$ and 2 are shown in Figure S8 (Supporting Information). One can see the length of the hydrogen bonds in the DJPs with $n_C = 2$ have the same trend with the interlayer spacings and formation energies, confirming the crucial role of the polarity of spacer cations. But for the DJPs with $n_C = 1$, there is an apparent deviation between the length of the hydrogen bonds and the formation energies, indicating the strong hydrogen bonds can no longer help stabilize the structure of the DJPs. Besides, from the lengths of the hydrogen bonds in Figure 2a and Figure S8 (Supporting Information), we can conclude that a spacer cation with a shorter chain length tends to bring about even stronger hydrogen bonds between the spacer cations and inorganic layers, which further proves the strong hydrogen bonds cannot guarantee high stability of the DJPs with $n_C = 1$. The distortion of the inorganic layers can be visually examined by the length of the six Pb—I bonds, marked from 1 to 6 in Figure S9 (Supporting Information). The lengths of the Pb—I bonds of all the DJPs with different chain lengths are listed in Tables S1–S5 (Supporting Information), where the largest and smallest values are marked red and pale blue, respectively. It is obvious that the octahedral distortion is reduced as the n_C value increases, which confirms that a spacer cation with a chain length that is too short can make the inorganic layers distorted. These results reveal that a spacer cation that is too short will distort the inorganic layers in DJPs. Still, a too-long one will weaken the hydrogen bonds between the organic spacer and inorganic layers. As a result, to obtain robust DJP materials, a spacer cation with an optimal chain length is also important.

Apart from the chain-like spacer cations studied in this work, there are also aromatic compound-based spacer cations. Similar to the chain-like spacer cations, the polarity and chain length of the aromatic compounds-based spacer cations are also supposed to influence the DJPs following the same roles as the chain-like ones. That aromatic compound can also be seen as one kind of branch chain of the molecule. Besides, the DJPs with the aromatic compounds-based spacer cations are supposed to have higher humidity stability because of their larger molecules. However, they also suffer from larger steric hindrance, which can distort the inorganic layers, leading to poor crystallinity and structure instability.

3. Conclusion

In conclusion, to figure out the influence of spacer cations' molecular structures on the structural and optoelectronic properties of DJPs, we detailly investigated a series of DJPs with different spacer cations through theoretical and experimental methods. We found that the polarity of the spacer cations plays a crucial role in determining the structure stability and optoelectronic properties of the DJPs. For the spacer cations with a large polarity component along the main chain direction, the high polarity can not only strengthen the hydrogen bonds between the organic spacer layers and inorganic octahedral layers but also create less distortion to the octahedral layers and shorten the interlayer spacings. All these promotions contribute to the high stability and superior optoelectronic properties of the DJPs. In addition, an optimal chain length of the spacer cations was found to be crucial to constructing ideal DJPs. A spacer cation that is too short or too long will weaken the lattice structures of the DJPs. These valuable findings will help people further cognize the role of spacer cations and discover more diverse and remarkable DJPs that assist their development and commercialization.

4. Experimental Section

Synthesis of Materials: The $DMPAPbI_4$ and $PDAPbI_4$ DJP precursors were prepared by dissolving $DMPAI_2$ ($PDAI_2$) and PbI_2 in dimethylformamide at a molar ratio of 1:1 to create a 1 M solution. The precursors were stirred in the glovebox for 4 h before use.

Film and Device Fabrication: The glass slides were ultrasonically cleaned sequentially with acetone, ethanol, and deionized water. They were then treated with an oxygen plasma to enhance hydrophilicity. Next, 40 µL of precursor solution was spin-coated onto the slides at 3000 rpm for 30 s, then thermal annealing at 100 °C for 10 min. Using shadow masks, 100-nm-thick Au electrodes were thermally evaporated onto the DJP films to fabricate the photodetectors. The photodetectors have a channel length of 10 µm and a width of 70 µm.

Film and Device Characterization: A Thermo Scientific ESCALAB 250Xi system was employed to perform the XPS measurement. The XRD patterns were obtained using a Bruker D2 Phaser with Cu Kα radiation. The film morphologies were characterized with a FEI Quanta 450 FEG SEM. Absorption spectra were recorded using a Hitachi UH 4150 UV–vis absorption spectrophotometer. The thermal stability of the films was assessed by TGA (PerkinElmer Simultaneous Thermal Analyzer 6000). The photodetection performance of the fabricated photodetectors was evaluated using a standard electrical probe station equipped with an Agilent 4155C semiconductor analyzer. A 405 nm laser served as the light source for photodetector measurements, with incident irradiation power measured by a PM400 power meter from Thorlabs.

Computational Details: The first-principles calculations were performed by the Vienna Ab initio Simulation Package (VASP) and the Cambridge Sequential Total Energy Package module in Material Studio software based on density functional theory (DFT).[36,37] The generalized-gradient approximation for exchange–correlation energy proposed by Perdew, Burke, and Ernzerhof was used.[38] The convergence criteria for the energy and atomic forces were set to 5×10^{-4} eV and 0.01 eV $Å^{-1}$, respectively. The Brillouin zone was sampled with $3 \times 3 \times 3$ *k* point meshes for structural optimization and denser $5 \times 5 \times 5$ *k* point meshes for the electronic and optical properties. The COHP and the ICOHP were calculated by the Local Orbital Basis Suite Towards Electronic-Structure Reconstruction (LOBSTER) program.[39] The DFT calculations for the polarity of the spacer molecules were performed using the Gaussian09 program package.[40] The geometry optimizations of the spacer cations were carried out at Becke's three-parameter functional and Lee-Yang-Parr functional (B3LYP) level of theory with the 6–31G (d, p) basis.[41,42]

Supporting Information

Supporting Information is available from the Wiley Online Library or from the author.

Acknowledgements

This work was supported by a fellowship award from the Research Grants Council of the Hong Kong Special Administrative Region, China (CityURFS2021-1S04) and the City University of Hong Kong (project no. 9229138).

Conflict of Interest

The authors declare no conflict of interest.

Data Availability Statement

The data that support the findings of this study are available from the corresponding author upon reasonable request.

Keywords

Dion–Jacobson, halide perovskite, optoelectronic, photodetector, spacer cation, stability

Received: June 8, 2024
Revised: July 18, 2024
Published online:

[1] B. Zhao, B. Guo, S. Xing, Z. Liu, Y. Yuan, Z. Ren, W. Tang, Y. Lian, G. Zhang, C. Zou, D. Di, *Matter.* **2024**, *7*, 772.
[2] H. Meng, K. Mao, F. Cai, K. Zhang, S. Yuan, T. Li, F. Cao, Z. Su, Z. Zhu, X. Feng, W. Peng, J. Xu, Y. Gao, W. Chen, C. Xiao, X. Wu, M. D. McGehee, J. Xu, *Nat. Energy.* **2024**, *9*, 536.
[3] S. Wu, Y. Yan, J. Yin, K. Jiang, F. Li, Z. Zeng, S. W. Tsang, A. K. Y. Jen, *Nat. Energy.* **2024**, *9*, 411.
[4] T. Zhu, X. Z. Lu, T. Aoyama, K. Fujita, Y. Nambu, T. Saito, H. Takatsu, T. Kawasaki, T. Terauchi, S. Kurosawa, A. Yamaji, H. B. Li, C. Tassel, K. Ohgushi, J. M. Rondinelli, H. Kageyama, *Nat. Mater.* **2024**, *23*, 182.
[5] K. Elkhouly, I. Goldberg, X. Zhang, N. Annavarapu, S. Hamdad, G. Croes, C. Rolin, J. Genoe, W. Qiu, R. Gehlhaar, P. Heremans, *Nat. Photonics.* **2024**, *18*, 132.
[6] W. Zhang, X. Guo, Z. Cui, H. Yuan, Y. Li, W. Li, X. Li, J. Fang, *Adv. Mater.* **2024**, 2311025.
[7] F. H. Isikgor, S. Zhumagali, L. V. Luis, M. De Bastiani, I. McCulloch, S. De Wolf, *Nat. Rev. Mater.* **2023**, *8*, 89.
[8] X. Lu, K. Sun, Y. Wang, C. Liu, Y. Meng, X. Lang, C. Xiao, R. Tian, Z. Song, Z. Zhu, M. Yang, Y. Bai, Z. Ge, *Adv. Mater.* **2024**, *36*, 2400852.
[9] S. Jiang, M. Liu, D. Zhao, Y. Guo, J. Fu, Y. Lei, Y. Zhang, Z. Zheng, *Phys. Chem. Chem. Phys.* **2024**, *26*, 4794.
[10] Y. Li, Y. Wang, Z. Xu, B. Peng, X. Li, *ACS Nano.* **2024**, *18*, 10688.
[11] T. Leijtens, G. E. Eperon, N. K. Noel, S. N. Habisreutinger, A. Petrozza, H. J. Snaith, *Adv. Energy Mater.* **2015**, *5*, 1500963.
[12] L. Etgar, *Energy Environ. Sci.* **2018**, *11*, 234.
[13] Z. Lai, Z. Zeng, Y. Meng, Y. Zhang, Y. Shen, W. Wang, D. Li, D. Chen, D. Yin, S. W. Tsang, S. P. Yip, J. C. Ho, *Adv. Funct. Mater.* **2023**, *33*, 2305539.

[14] P. Kour, M. C. Reddy, S. Pal, S. Sidhik, T. Das, P. Pandey, S. P. Mukherjee, S. Chakraborty, A. D. Mohite, S. Ogale, *Angew. Chem., Int. Ed.* **2021**, *77005*, 18750.
[15] C. M. M. Soe, C. C. Stoumpos, M. Kepenekian, B. Traoré, H. Tsai, W. Nie, B. Wang, C. Katan, R. Seshadri, A. D. Mohite, J. Even, T. J. Marks, M. G. Kanatzidis, *J. Am. Chem. Soc.* **2017**, *139*, 16297.
[16] W. Ke, L. Mao, C. C. Stoumpos, J. Hoffman, I. Spanopoulos, A. D. Mohite, M. G. Kanatzidis, *Adv. Energy Mater.* **2019**, *9*, 1803384.
[17] S. Ahmad, P. Fu, S. Ahmad, P. Fu, S. Yu, Q. Yang, X. Liu, X. Wang, X. Wang, *Joule.* **2018**, *3*, 794.
[18] W. Guo, Z. Yang, J. Dang, M. Wang, *Nano Energy.* **2021**, *86*, 106129.
[19] M. Liu, T. Pauporté, *Nano-Micro Lett.* **2023**, *15*, 134.
[20] T. Niu, H. Ren, B. Wu, Y. Xia, X. Xie, Y. Yang, X. Gao, Y. Chen, W. Huang, *J. Phys. Chem. Lett.* **2019**, *10*, 2349.
[21] D. Xin, M. Zhang, Z. Fan, Y. Yang, S. Dong, L. Lei, W. Zhao, Q. Lin, X. Zheng, *Adv. Funct. Mater.* **2024**, 2402480.
[22] D. Xin, M. Zhang, Z. Fan, N. Yang, R. Yuan, B. Cai, P. Yu, J. Zhu, X. Zheng, *J. Phys. Chem. Lett.* **2022**, *13*, 11928.
[23] T. Yang, C. Ma, W. Cai, S. Wang, Y. Wu, J. Feng, N. Wu, H. Li, W. Huang, Z. Ding, L. Gao, S. (Frank) Liu, K. Zhao, *Joule.* **2023**, *7*, 574.
[24] P. Fu, M. A. Quintero, E. S. Vasileiadou, P. Raval, C. Welton, M. Kepenekian, G. Volonakis, J. Even, Y. Liu, C. Malliakas, Y. Yang, C. Laing, V. P. Dravid, G. N. M. Reddy, C. Li, E. H. Sargent, M. G. Kanatzidis, *J. Am. Chem. Soc.* **2023**, *145*, 15997.
[25] P. Fu, M. A. Quintero, C. Welton, X. Li, B. Cucco, M. C. De Siena, J. Even, G. Volonakis, M. Kepenekian, R. Liu, C. C. Laing, V. Klepov, Y. Liu, V. P. Dravid, G. N. Manjunatha Reddy, C. Li, M. G. Kanatzidis, *Chem. Mater.* **2022**, *34*, 9685.
[26] Y. Shen, S. Hu, Y. Meng, S. P. Yip, J. C. Ho, *Mater. Today Electron.* **2024**, *8*, 100100.
[27] J. Even, C. Katan, C. C. Stoumpos, R. D. Schaller, M. G. Kanatzidis, **2019**, *141*, 12880.
[28] Y. Qin, H. Zhong, J. J. Intemann, S. Leng, M. Cui, C. Qin, M. Xiong, F. Liu, A. K. Y. Jen, K. Yao, *Adv. Energy Mater.* **2020**, *10*, 1904050.
[29] R. Dronskowski, M. Festkbrperforschung, P. E. Blochl, *J. Phys, Chem.* **1993**, *97*, 8617.
[30] H. Yao, Z. Li, C. Shi, Y. Xu, Q. Wang, Z. H. Li, G. Peng, Y. Lei, H. Wang, Z. Ci, Z. Jin, *Adv. Funct. Mater.* **2022**, *32*, 2205029.
[31] T. Liu, J. Guo, D. Lu, Z. Xu, Q. Fu, N. Zheng, Z. Xie, X. Wan, X. Zhang, Y. Liu, Y. Chen, *ACS Nano.* **2021**, *15*, 7811.
[32] Y. Fu, *Adv. Mater.* **2022**, *34*, 2108556.
[33] S. Yu, M. Abdellah, T. Pullerits, K. Zheng, Z. Liang, *Adv. Funct. Mater.* **2021**, *31*, 2104342.
[34] J. Even, L. Pedesseau, C. Katan, *ChemPhysChem.* **2014**, *15*, 3733.
[35] M. E. Kamminga, H. H. Fang, M. R. Filip, F. Giustino, J. Baas, G. R. Blake, M. A. Loi, T. T. M. Palstra, *Chem. Mater.* **2016**, *28*, 4554.
[36] G. Kresse, J. Furthmüller, *Phys. Rev. B Condens. Matter Mater. Phys.* **1996**, *54*, 11169.
[37] S. J. Clark, M. D. Segall, C. J. Pickard, P. J. Hasnip, M. I. J. Probert, K. Refson, M. C. Payne, *Zeitschrift fur Krist.* **2005**, *220*, 567.
[38] J. P. Perdew, K. Burke, M. Ernzerhof, *Phys. Rev. Lett.* **1996**, *77*, 3865.
[39] V. L. Deringer, A. L. Tchougréeff, R. Dronskowski, *J. Phys. Chem. A.* **2011**, *115*, 5461.
[40] M. J. Frisch, G. W. Trucks, H. B. Schlegel, G. E. Scuseria, M. A. Robb, J. R. Cheeseman, G. Scalmani, V. Barone, B. Mennucci, G. A. Petersson, H. Nakatsuji, M. Caricato, X. Li, H. P. Hratchian, A. F. Izmaylov, J. Bloino, G. Zheng, J. L. Sonnenberg, M. Hada, M. Ehara, K. Toyota, R. Fukuda, J. Hasegawa, M. Ishida, T. Nakajima, Y. Honda, O. Kitao, H. Nakai, T. Vreven, J. A. Montgomery, et al., *Gaussian 09, Revision D. 01*, Gaussian. Inc., Wallingford, CT, USA **2009**.
[41] T. Lecklider, *EE Eval. Eng.* **2011**, *50*, 36.
[42] A. D. Becke, *J. Chem. Phys.* **1992**, *96*, 2155.